HAL
open science

Decadal to monthly timescales of magma transfer and reservoir growth at a caldera volcano

Timothy H. Druitt, Fidel Costa Rodriguez, M. Dungan, Bruno Scaillet

To cite this version:

Timothy H. Druitt, Fidel Costa Rodriguez, M. Dungan, Bruno Scaillet. Decadal to monthly timescales of magma transfer and reservoir growth at a caldera volcano. Nature, 2012, 482, pp.77-82. 10.1038/nature10706 . insu-00666208

HAL Id: insu-00666208

https://insu.hal.science/insu-00666208v1

Submitted on 6 Jul 2012

HAL is a multi-disciplinary open access archive for the deposit and dissemination of scientific research documents, whether they are published or not. The documents may come from teaching and research institutions in France or abroad, or from public or private research centers.

L'archive ouverte pluridisciplinaire **HAL**, est destinée au dépôt et à la diffusion de documents scientifiques de niveau recherche, publiés ou non, émanant des établissements d'enseignement et de recherche français ou étrangers, des laboratoires publics ou privés.

Decadal to monthly timescales of magma transfer and reservoir growth at a caldera volcano

T.H. Druitt[1,2,3], F. Costa[4], E. Deloule[5], M. Dungan[6] & B. Scaillet[7]

1 Clermont Université, Université Blaise Pascal, Laboratoire Magmas et Volcans, BP 10448, F-63000 Clermont-Ferrand, France
2 CNRS, UMR 6524, LMV, F-63038 Clermont-Ferrand, France
3 IRD, R 163, LMV, F-63038, Clermont-Ferrand, France
4 Earth Observatory of Singapore, Nanyang Technological University, Singapore
5 CRPG-CNRS, BP20, 54501 Vandoeuvre les Nancy, France
6 Département de Minéralogie, Université de Genève, Rue des Maraîchers 13 CH-1205 Genève, Switzerland
7 ISTO - UMR 6113 CNRS / Université d'Orléans/Université Francois Rabelais de Tours, 1A rue de la Ferollerie, 45071 Orleans, France

Caldera-forming volcanic eruptions are low-frequency, high-impact events capable of discharging tens to thousands of cubic kilometres of magma explosively on timescales of hours to days, with devastating effects at local and global scales[1]. Since no such eruptions have been monitored during the long build-up phase, the precursor phenomena are not well understood. Interpretations of geophysical signals obtained during recent episodes of caldera unrest are difficult to interpret, and not all periods of unrest culminate in eruptions[2,3]. We have studied pre-eruptive magmatic processes and their timescales using chemically zoned crystals from the late 17th century BC 'Minoan' caldera-forming eruption of Santorini Volcano, Greece[4]. The results provide insights into how rapidly large silicic systems may pass from a quiescent state to one perched on the edge of eruption[5,6]. Despite the large volume of magma erupted (40-60 km^3)[4], and the 18,000-year gestation period since the last major eruption, most crystals in the Minoan magma record processes that are <~100 years old. Recharge of the magma reservoir by silicic magma occurred during the century prior to eruption, with mixing between different silicic magma batches still taking place during the final months. Large silicic magma reservoirs may apparently be emplaced on timescales that are geologically very short compared to the preceding repose period, with major growth phases immediately before eruption. These observations have implications for monitoring strategies and responses to unrest at long-dormant, but potentially active, caldera systems such as Yellowstone or Campi Flegrei[2].

Crystals in volcanic rocks provide records of magma-reservoir processes and timescales prior to eruptions[7]. A crystal growing from a magmatic melt incorporates trace elements in quantities governed by thermodynamic and kinetic laws[8,9]. If the crystal is subsequently mixed into another melt, trace elements that

diffuse sufficiently fast will begin to re-equilibrate with the new host melt, generating intra-crystalline diffusion gradients than can be used to obtain time information[10-12] (Supplementary Fig. S1).

A novel technique for extracting multiple timescales from single crystals has been applied to plagioclase crystals in rhyodacitic (71-72 wt% SiO_2) pumices from the Minoan eruption. The pumices from all four phases of the eruption (1. plinian; 2 and 3. phreatomagmetaic; 4. ignimbrite[13]) contain ~10 vol% crystals set in rhyolitic (73-74 wt% SiO_2)[13] glass. Plagioclase is the dominant crystalline phase, the others being orthopyroxene, clinopyroxene, magnetite, ilmenite and apatite. It occurs as zoned crystals, whose compositional variations are dominated by charge-coupled solid solution between the end-members anorthite (An – $CaAl_2Si_2O_8$) and albite ($NaAlSi_3O_8$).

Two types of plagioclase have been recognized from examination of 300 crystals (Fig. 1; Figs. S2 and S3). A dominant type (type 1) has a euhedral to partly resorbed core of An_{58-43} overgrown by a variably developed, euhedral rim of An_{43-36} containing multiple dissolution surfaces (Figs. 1a-d). The cores and rims form compositionally distinct populations (Fig. 1g). In some crystals, the core also contains a euhedral to anhedral inner core of An_{88-58} ('calcic inner core'; Fig 1 a, c). A spectrum of type 1 crystals is observed from those with thick rims (up to 100 μm), to those with thin rims, to those in which the rim is absent (Fig. 1f). In rimmed type 1 crystals the plagioclase in contact with the host glass is ~ $An_{40,}$ whereas in rimless ones it is ~An_{50} (i.e., the core composition). Rimmed type-1 crystals occur in pumices from all four eruptive phases, but rimless ones have only been observed in pumices from phase 4. Type 2 crystals are very rare; they are reversely zoned, with cores of An_{36-30} mantled by rims identical to those of type 1 (Fig. 1e). The broad range of plagioclase compositions in Minoan pumice shows that the rhyodacite was the product of open-system magmatic processes involving multiple, compositionally diverse magmas.

Trace elements were analysed in four rimmed type-1 crystals, one rimless type-1 crystal, some interstitial glasses and some inclusions of glass contained within the crystals (Fig. 2; Tables S1 and S2). Mg, Sr and Ti are particularly useful elements for characterizing coexisting melt compositions and mixing time scales because they partition differently between melt and plagioclase[8] and diffuse at different rates. Mg diffuses faster than Sr[7]; Ti probably diffuses slowly due to its high charge. Published An-dependent partition coefficients[8] were used to invert melt trace element contents to those of equivalent plagioclase (Fig. 2), and vice versa (Fig. 3). Rimmed type-1 crystals have core-to-rim gradients in all the three elements (Fig. 2). Rim compositions record equilibrium with the interstitial glass, but concentrations of Mg, Sr, and Ti in the cores and calcic inner cores are significantly higher than those calculated to be in equilibrium with the glass (green lines, Fig. 2). The rimless type-1 crystal has concentrations of Mg and Sr throughout that are too high to have been in equilibrium with the glass. None of these crystals resided in the host melt long enough for any of these the elements to reach total equilibrium with the host melt.

This observation is reinforced by a comparison of calculated Mg, Ti, and Sr concentrations of melts in equilibrium with the different plagioclase zones (referred to as Mg_{melt}, Sr_{melt}, and Ti_{melt}), with those of Santorini lavas, pumices, and glasses. The latter represent an approximate liquid line of descent of the magmatic system

(Fig. 3a, b). The calculated concentrations of Sr_{melt} and Ti_{melt} span the entire range of erupted compositions, whereas those of Mg_{melt} fall below the liquid line of descent, especially in the calcic inner cores. The crystals retain near-primary values of Sr and Ti, but Mg appears to have been partially re-equilibrated by diffusion.

The Sr contents of the crystals were used to calculate the compositions of melts from which the different zones had crystallized (Fig. 3). The rims of the type-1 and type-2 crystals formed from melts with 60-90 ppm Sr (71-74 % SiO_2), which encompasses the range of whole-rock to glass compositions of the host rhyodacite. The cores of the type-1 crystals formed from melts with 110-170 ppm Sr (dacite with 63-69 % SiO_2), and the cores of the type-2 crystals formed from melts with 40-60 ppm Sr (rhyolite with 74-76 wt % SiO_2). We interpret these observations as recording the mixing of a dacite (carrying plagioclase of the type-1 core composition) with a rhyolite (carrying rare plagioclase of the type-2 core composition) to generate a hybrid rhyodacite (followed by growth of the rim) that was erupted as the Minoan pumice. The rimless type-1 crystals were derived directly from the dacite, and had not resided in the hybrid rhyodacite long enough to grow rims. The calcic inner cores formed from basaltic-andesite melts with >200 ppm Sr and <57 % SiO_2 that were mixed into the dacite at an early stage.

The times elapsed between the different mixing events and eruption have been calculated by modelling the partial relaxation of Mg concentrations in different parts of the crystals[12] (Fig. 2; Table 1). We first modelled the entire crystal ('1-step model'), which assumes that diffusion started only after the crystal had grown. Model results ranged from 1 to 60 years, but good fits could not be obtained. We therefore approximated the more realistic situation of simultaneous crystal growth and diffusion by modelling the crystals incrementally zone by zone ('2-step model'). In this manner we obtained better overall fits to the data (Fig. 2), from which we infer that: (1) a first magma mixing episode recorded by incorporation of the calcic inner cores of the type-1 crystals into the dacite occurred no more than ~100 years prior to eruption; (2) a second mixing episode, or series of episodes, involving the dacite and the rhyolite occurred less than ~10 years prior to eruption; (3) the rimless type-1 crystals cannot have resided in the Minoan magma more than a few months without some diffusive loss of Mg from the rim. We have no constraints on the ages of the cores of the rare type-2 crystals. The estimates are robust to better than an order of magnitude (Methods section). The Mg-derived times were tested against the diffusive equilibration of Sr using the comprehensive diffusion data for this element (Fig. 2). Taking the measured profiles of Sr as being close to initial values, diffusion times an order of magnitude longer than those obtained from Mg would significantly blur the observed tight correlation between Sr and An contents (Fig. 3c), and are ruled out.

Our interpretation, which is justified more fully in the Supplementary Discussion, is as follows. During the century prior to eruption, dacitic magma containing crystals of calcic plagioclase began to ascend from a deep storage zone beneath Santorini, possibly pushed by injections of mafic magma (Fig. S4). Once at shallow levels, the dacite intersected one or more extant bodies of rhyolite situated at a few km depth[14]. The cores of the type-1 crystals grew during ascent of the dacite, and/or ponding of it at the base of the reservoir. Then, starting about a decade prior the eruption, the dacite mixed with the rhyolite, forming rim overgrowths on those crystals.

Mixing caused resorption of most crystals initially present in the rhyolite, and formed the hybrid rhyodacite that was subsequently erupted. Successive waves of dacitic recharge and heating of the reservoir are recorded as multiple dissolution surfaces within the crystal rims. Dacite was still being mixed into the shallow reservoir less than a few months before eruption occurred, supplying the rimless type-1 crystals. Efficient mixing of the two silicic magmas on these timescales is compatible with fluid dynamics principles (Supplementary Discussion). Basaltic andesite was also injected at a late stage, accounting for small quantities of scoria discharged during the first eruptive phase[13]. The resident rhyolite must have been more radiogenic than the dacite, since Minoan plagioclase crystals have lower Sr isotopic ratios than their host glass[15]. The rhyolite had probably been crustally contaminated during residence at high crustal levels. The dacite may have been a vanguard batch of the magmas that have erupted over the last 2000 years to form the postcaldera Kameni Islands[13]. This interpretation is based on similarities in An and Sr contents between the cores of type-1 plagioclases and those of plagioclases in the postcaldera lavas[16,17] (Figs. 1 and 3).

Calculations based on chemical mass balance and crystal content show that the dacite accounted for at least 15 % of the hybrid rhyodacite (Supplementary Discussion). We conservatively conclude that the Minoan reservoir increased its volume by at least a few km^3 in the last century prior to eruption (corresponding to an intrusion rate of >0.05 km^3/y), accommodated by some combination of roof flexure, lateral intrusion and reservoir-floor subsidence[18,19]. This timescale is very short compared to the 18,000-y gestation period since the previous major explosive eruption of Santorini[13], suggesting that the Minoan reservoir was a transient feature on geological timescales[14,20,21].

Our study has important implications for the recognition and interpretation of precursor signals prior to caldera-forming eruptions. It shows that shallow bodies of silicic magma may be emplaced rapidly beneath caldera systems following long periods of dormancy, with significant growth phases still taking place in the final months before eruption. Even our conservative estimate of magma recharge rate prior to the Minoan eruption exceeds those measured at historically restless caldera systems that have not resulted in eruptions (typically ~0.01 km^3/y)[2,3], suggesting that particularly high and sustained rates may be necessary to trigger eruptions in such systems[22]. Indeed evidence is emerging of large recharge events involving magmas of a wide range of compositions, in the decades to months leading up to other large explosive eruptions[11,23-25]. Long-term monitoring of large, dormant caldera systems is essential in order to ensure detection of geophysical and geochemical signals resulting from these processes during the possibly short-lived build-up to caldera-forming eruptions.

METHODS SUMMARY

The zoning textures of about 300 crystals from eight pumices (from all four eruptive phases) were studied using a combination of back-scattered electron microscopy and Normarski differential interference contrast microscopy. Major element compositions of minerals and glasses were analyzed by electron microprobe, and trace elements by secondary ion mass spectrometry. The pre-eruptive temperature of the

Minoan rhyodacite (853±12 °C) was calculated using analyses of touching magnetite-ilmenite pairs in pumices from all eruptive phases, the recalculation procedure of ref. 26, and the thermometer of ref. 27.

Trace element diffusion modelling was carried out in one dimension using a forward modelling approach in which the diffusion equation[12] was solved numerically by a finite difference scheme, and visual best-fits were made between modelled and observed concentration profiles. The An-dependent diffusion coefficient for Mg was taken from ref. 12, based on the experimental data of ref. 28, and that for Sr was taken from ref. 29. Initial profiles for Mg were calculated using the Sr-An correlation of Fig. 3c, along with the Mg-Sr liquid line of descent (Fig. 3b). The boundary conditions were determined by the measured concentrations at the crystal rims or at other major boundary zones. The calculated times are probably overestimates because some of the cores have re-equilibrated significantly, so that the effect of diffusion in multiple dimensions could have been significant[7]. However, the main errors associated with the calculations arise from uncertainties of temperature and diffusion coefficients. The modelling was carried out at either 855 or 900 °C, depending on the melt involved (Table 1), but we considered a nominal uncertainty of ±25 ^{o}C, which when propagated onto the time estimates leads to relative errors of 45-75 % (Table 1). Effects of uncertainties in the diffusion parameters for Mg are discussed in the Methods section.

References

1. Miller, C.F. & Wark, D.A. Supervolcanoes and their explosive supereruptions. *Elements* **4**, 11-16 (2008).
2. Newhall, C.G. & Dzurizin, D. Historical unrest at large calderas of the world. U.S. Geol. Surv. Bull. **1855**, 1108 pp (1988).
3. Gottsmann, J. & Marti, J. Caldera volcanism: analysis, modelling and response. *Developments in Volcanology* **10**, Elsevier, 492 pp (2008).
4. Sigurdsson H, Carey S & 12 others. Marine investigations of Greece's Santorini volcanic field. *EOS* **87**: 337-342 (2006).
5. Bachmann, O. & Bergantz, G.W. On the origin of crystal-poor rhyolites: Extracted from batholithic crystal mushes. *J. Petrol.* **45**, 1565-1582 (2004).
6. Burgisser, A. & Bergantz, G.W. A rapid mechanism to remobilize and homogenize highly crystalline magma bodies. *Nature* **471**, 212-215 (2011).
7. Costa, F., Dohmen, R. & Chakraborty S. Timescales of magmatic processes from modeling the zoning patterns of crystals. *Rev. Mineral. Geochem.* **69**, 545-594 (2008).
8. Bindeman, I.N., Davis, A.M. & Drake, M.J. Ion microprobe study of plagioclase-basalt partition experiments at natural concentration levels of trace elements. *Geochim. Cosmochim. Acta* **62**, 1175-1193 (1998).
9. Blundy, J. & Wood, B. Crystal-chemical control on the partitioning of Sr and Ba between plagioclase feldspar, silicate melts, and hydrothermal solutions. *Geochim. Cosmochim. Acta* **55**, 193-209 (1991).
10. Zellmer, G.F., Blake, S., Vance, D., Hawkesworth, C. & Turner, S. Plagioclase residence times at two island arc volcanoes (Kameni Islands, Santorini, and Soufriere, St Vincent) determined by Sr diffusion systematics. *Contrib. Mineral. Petrol.* **136**, 345-357 (1999).
11. Morgan, D.J., Blake, S., Rogers, N.W., De Vivo, B., Rolandi, G. & Davidson, J. Magma chamber recharge at Vesuvius in the century prior to the eruption of A.D. 79. *Geology* **34**, 845-848 (2006).
12. Costa, F., Chakraborty, S. & Dohmen, R. Diffusion coupling between trace and major elements and a model for calculation of magma residence time using plagioclase. *Geochim. Cosmochim. Acta*, **67**, 2189-2200 (2003).
13. Druitt, T.H., Edwards, L., Mellors, R.M., Pyle, D.M., Sparks, R.S.J., Lanphere, M., Davies, M. &

Barreiro, B. Santorini Volcano. *J. Geol. Soc. Lond. Memoirs* **19**, 165pp (1999).
14. Cottrell, E., Gardner, J.E. & Rutherford, M.J. Petrologic and experimental evidence for the movement and heating of the pre-eruptive Minoan rhyodacite (Santorini, Greece). *Contrib. Mineral. Petrol.* **135**, 315-331 (1999).
15. Martin, V., Davidson, J., Morgan, D. & Jerram, D. Using the Sr isotope compositions of feldspars and glass to distinguish magma system components and dynamics *Geology*, **38**, 539-542 (2010).
16. Francalanci, L., Vougioukalakis, G., & 5 others. Petrographic, chemical and isotopic variations in the intra-caldera post-Minoan rocks of the Santorini volcanic field. *Proceedings of the second workshop, Santorini, Greece, European Commission* pp175-186 (1998).
17. Huijsmans, J. Calc-alkaline lavas from the volcanic complex of Santorini, Aegean Sea, Greece. *Geologica Ultraiectina* 41, 316 pp (1985).
18. Pitcher, W.S. & Bussell, M.A. Structural control of batholithic emplacement in Peru: a review. *J. Geol. Soc. Lond.* **133**, 249-255 (1977).
19. Grocott, J., Arévalo, C., Welkner, D. & Cruden, A. Fault-assisted vertical pluton growth: Coastal Cordillera, north Chilean Andes. *J. Geol. Soc. Lond.* **166**, 295-301 (2009).
20. Glazner, A.F., Bartley, J.M., Coleman, D.S., Gray, W. & Taylor, R.Z. Are plutons assembled over millions of years by amalgamation from small magma chambers? *GSA Today* **14**, 4-11 (2004).
21. Annen, C. From plutons to magma chambers. Thermal constraints on the accumulation of eruptible silicic magma in the upper crust. *Earth Planet. Sci. Lett.* **284**, 409-416 (2009).
22. Jellenik, A.M. & DePaulo, D.J. A model for the origin of large silicic magma chambers: precursors of caldera-forming eruptions. *Bull. Volcanol.* **65**, 363-381 (2003).
23. Wark, D.A., Hildreth, W., Spear, F.S., Cherniak, D.J. & Watson, E.B. Pre-eruption recharge of the Bishop magma system. *Geology* **35**, 235-238 (2007).
24. Saunders, K.E., Morgan, D.J., Baker, J.A. & Wysoczanski, R.J. The magmatic evolution of the Whakamaru supereruption, New Zealand, constrained by a microanalytical study of plagioclase and quartz. *J. Petrol.* **51**, 2465-2488 (2010).
25. De Silva, S., Salas, G. & Schubring, S. Triggering explosive eruptions – The case for silicic magma recharge at Huaynaputina, southern Peru. *Geology* **36**, 387-390 (2008).
26. Stormer, Jr. J.C., The effects of recalculation on estimates of temperature and oxygen fugacity from analyses of multicomponent iron-titanium oxides. *Amer. Mineral.* **68**, 586–594 (1983).
27. Andersen, D.J. & Lindsley, D.H., New (and final!) models for the Ti-magnetite/ilmenite geothermometer and oxygen barometer. *Eos Transactions. American Geophysical Union* **66**, 416 (1985).
28. LaTourette, T. & Wasserbourg, G.J. Mg diffusion in anorthite: implications for the formation of early solar system planetismals. *Earth Planet. Sci. Lett.* **158**, 91-108 (1998).
29. Giletti, B.J. & Casserly, J.E.D. Strontium diffusion kinetics in plagioclase feldspars. *Geochim. Cosmochim. Acta* **58**: 3785-3797 (1994).
30. Santo, A.P. Magmatic evolution processes as recorded in plagioclase phenocrysts of Nea Kameni rocks (Santorini Volcano, Greece). *Developments in Volcanology* **7**, 139-160 (2005).

Table 1. Times obtained by diffusion modelling of Mg in Minoan plagioclase

Pumice sample	Erup phase	Crystal (& type)	Times (years), 1-step model 900 °C	Times (years), 2-step model CIC-dm 900 °C	CIC-C-dm 900 °C	CIC-C-R-rm 855 °C	CIC-R-rm 855 °C	C-rm 855 °C	C-R-rm 855 °C
S82-30A	1	12 (rimmed 1)	47^{+38}_{-20}		70^{+56}_{-30}	12^{+10}_{-5}			
S82-34B	2	A2 (rimmed 1)	$0.8^{+0.6}_{-0.3}$					$0.6^{+0.5}_{-0.3}$	$0.3^{+0.3}_{-0.1}$
R2C	3	B3 (rimmed 1)	60^{+48}_{-26}	60^{+48}_{-26}			$< 0.9^{+0.8}_{-0.4}$		
S82-11D	4	A6 (rimmed1)	24^{+20}_{-10}		22^{+17}_{-9}	$0.9^{+0.8}_{-0.4}$			
S82-11D	4	A5 (rimless 1)						$< 0.3^{+0.3}_{-0.1}$	

CIC – calcic inner core, C - core, R - rim, dm – dacitic melt, rm – rhyodacitic melt. The calculations were done at the temperatures shown, which correspond to those of dacitic and rhyodacitic melts. The quoted errors correspond to a temperature uncertainty of $\pm$25 ^{o}C on the calculated time.

FIGURE CAPTIONS

Figure 1 | Images and compositions of plagioclase crystals in Minoan pumice. a-b Back-scattered electron images of two rimmed type-1 crystals (S82-30A 12 and S82-34B A2). **c-f** Sketches of representative plagioclase crystals of the different types (**c**: S82-30A 12; **d**: S82-34B A2; **e**: S82-20D 76; **f**: S82-20D C1). More crystals are shown in Fig. S2 of the Supplementary Information. **g** Histogram of Minoan plagioclase compositions, based on 922 analyses, showing the different compositional groups. A histogram of plagioclase compositions from the postcaldera lavas[16,17] is shown for comparison.

Figure 2 | Concentration-distance profiles of An (red dots) and of Sr, Ti and Mg (black dots) in Minoan plagioclase crystals (error bars $\pm$1 σ). Equilibrium profiles for Sr, Ti and Mg (green lines) were calculated using published partition functions[8] at 855 °C. Calculated plagioclase compositions in equilibrium with interstitial glass (ig), glass inclusion (gi) and whole-rock (wr) pumice compositions[13] are also shown. Initial Mg profiles are the blue lines (with 1σ range). The red solid lines on the Mg plot are the best-fit 2-step Mg diffusion models (time shown in years). The red dotted lines on the Sr plots are diffusion models (1-step models; 900 °C; time shown in years) assuming that the measured profile is close to the initial condition as suggested by Fig. 3a. They show that times an order of magnitude longer than those derived from Mg would be inconsistent with the observed correlation between Sr and An contents (Fig. 3c).

Figure 3 | Melt compositions calculated by inversion of plagioclase trace element compositions. **a-b** Ti, Mg and Sr melt contents calculated using the plagioclase-liquid partition functions of ref. 8. Temperature was obtained from T (°C) = 855 + 200.(%An-40)/(80-40), which assumes that An_{40} plagioclase crystallized at 855 °C

and An_{80} crystallized at 1055 °C, the temperature of Santorini basaltic andesite. The values are compared with the compositional fields of Santorini cycle-2 lavas[17], Minoan pumice and Minoan glasses. The range of Mg_{melt} values calculated in the same way from the Mg contents of calcic (An>80) plagioclase in Santorini basalts and basaltic andesites are much higher (14000-47000 ppm) than those in the calcic inner cores of Minoan crystals, showing that the latter have lost Mg by diffusion. **c-d** Use of calculated melt Sr contents from plagioclase enables estimation of the SiO_2 contents of the melts from which each plagioclase compositional group crystallized. The compositional field of plagioclases in the postcaldera lavas is taken from ref. 30.

Supplementary Information.

Six additional figures, details of analytical and modelling methods, tables of trace element data for plagioclases and glasses and discussions of data and interpretations.

Acknowledgements

This study was funded partly by the French Agence National de Recherche (ANR STOMIXAN, Contract No ANR-08CEA080 to B. Scaillet). We are grateful to Robin Armstrong, Pierre Crançon and Rachel Girardin for their contributions during the early stages of this study, and to Jon Blundy and Mary Reid for helpful reviews.

Author contributions. T.D. defined the project strategy, analysed the data, and wrote the first draft of the manuscript, which was then revised by all the authors. E.D., MD. and T.D. made the trace element analyses, F.C. did the diffusion modelling, and BS applied the fluid dynamic principles.

Author information. Correspondence and requests for materials should be addressed to T.D. (T.Druitt@opgc.univ-bpclermont.fr).

METHODS

Sample preparation and analysis

Plagioclase crystals (250-400 and 400-700 μm size fractions) from eight pumices from all four eruptive phases[13] were mounted in epoxy resin, mostly on (010), then polished. The zoning textures of about 300 crystals were studied using a combination of back-scattered electron microscopy and Normarski differential interference contrast microscopy. Sectioning through the centres of the crystals was maximized by visual observation using a binocular microscope, and by rejection of zoning images that were evidently oblique cuts. Major element compositions of plagioclase were analyzed using a Cameca SX100 electron microprobe at an accelerating voltage of 15-20 kV and beam current of 8-15 nA.

Abundances of a number of isotopes up to ^{140}Ce, including ^{24}Mg, ^{47}Ti and ^{88}Sr, were analysed using two ion probes: a Cameca IMS 4f instrument at the University of Edinburgh (4.5-5 nA primary O- beam) and a Cameca IMS 1280 instrument at the CRPG, Nancy (14-20 nA primary O- beam) using beam diameters of 10-15

μm and calibrated against glass standards NBS 6104 and ML3B-G. Secondary ions were energy filtered using bandpasses of 100 V and 35 V, offsets of 100 V and 60 V, and mass resolutions of 300 and 5000 on the IMS 4f and the IMS 1280 respectively, following a short pre-sputtering period. Only high-energy ions were measured in order to reduce the matrix effect on relative ion yields[31]. The calibration line for Sr, including glass standards StHs, KL2G, TIG BHVO and BCR2G, and CRPG reference albite and plagioclase, display no matrix effect for a large range of glass and mineral compositions. Isotope concentrations were expressed as ratios relative to ^{30}Si, then corrected using electron microprobe analyses of Si contents adjacent to the ion probe pits. The relative ionisation yields were determined on glass standards. Internal precisions (mean relative deviation) on the ion/^{30}Si ratios for each spot analysis were typically better than 5% for Mg, 5% for Sr, and 10% for Ti. Values for all elements on the IMS 4f were systematically slightly lower than those on the IMS 1280, and were raised using a small multiplication factor.

Selected profiles were also analysed for Mg using a Cameca SX100 electron microprobe (accelerating voltage 15 kV; beam current 40 nA; total counting time per spot 50 s), and using a LA-ICP-MS system consisting of a 193 nm excimer (ArF) laser-ablation system (M50, Resonetics) coupled to an Agilent 7500CS ICP-MS (10 μm beam size; 6 mJ beam energy; 1Hz repetition rate). Results from the three techniques agreed to within + 25 %.

Crystal-melt trace element partitioning

We used the An-dependent partition functions of ref. 8 for Mg, Sr and Ti. The Sr partition function of ref. 9 gives results within a few percent of that of ref. 8. The partition functions for Mg, Sr and Ti of ref. 8 seem to work quite well for Santorini compositions. There is good agreement between the contents of Sr and Ti in the crystal rims and the plagioclase compositions calculated to be in equilibrium with the interstitial glasses (Fig. 2). Agreement for Mg is not as good, although the disparity is small compared to the overall range of this element in Santorini plagioclases and melts (Figs. 2 and 3b). Sr and Ti contents of the calcic inner cores of Minoan plagioclase crystals agree with those predicted by ref 8 to be in equilibrium with Santorini basaltic and basaltic andesite melts (Fig. 3a). Mg contents of calcic plagioclase occurring in Santorini basalts and basaltic andesites[32-34] agree with the Mg contents of those rocks (Fig. 3b) using the Mg partition coefficient of ref 8.

Diffusion modelling

Diffusion modelling was carried out using the method of ref. 12 with distance increments of 3.5-5.3 μm. We used the Mg diffusion coefficient in plagioclase of ref. 12, which is based on the experimental data of ref. 28.

$$D_{Mg} = \left[2.92 \times 10^{(-4.1XAn-3.1)} \exp\left(\frac{-266000}{RT}\right) \right] \qquad [S1]$$

The diffusion coefficient for Sr was taken from ref. 29.

$$D_{Sr} = \left[2.92 \times 10^{(-4.1XAn-4.08)} \exp\left(\frac{-276000}{RT}\right) \right] \qquad [S2]$$

where D is the element diffusion coefficient in m^2s^{-1}, *XAn* is the mol fraction of anorthite, and T is the temperature in Kelvin. From these equations, $D_{Mg}>D_{Sr}$ at all temperatures in plagioclase of a given An content. We used the equation for trace element diffusion in plagioclase derived in ref. 12, which takes into account the effect of An content on equilibrium profile shapes and diffusion coefficients,

$$\frac{\partial C_i}{\partial t} = \left(D_i \frac{\partial^2 C_i}{\partial x^2} + \frac{\partial C_i}{\partial x}\frac{\partial D_i}{\partial x}\right) - \frac{A}{RT}\left(D_i \frac{\partial C_i}{\partial x}\frac{\partial X_{\mathrm{An}}}{\partial x} + C_i \frac{\partial D_i}{\partial x}\frac{\partial X_{\mathrm{An}}}{\partial x} + D_i C_i \frac{\partial^2 X_{\mathrm{An}}}{\partial x^2}\right) \qquad [S3]$$

where *A* is a thermodynamic factor that relates the dependence of the partition coefficient on the An content[8], *x* is distance, *C* is concentration, and *t* is time.

We used two temperatures in the modelling: 900 °C for models in which the host melt was dacitic, and 855 °C for those in which it was rhyodacitic (Table 1). These temperatures are constrained by the 855 °C temperature of the magma on eruption (from touching pairs of Fe-Ti oxides), and are consistent with the formula used for plagioclase-melt element partitioning (legend of Fig. 3).

The *equilibrium* distributions of Mg, Sr and Ti within the plagioclase crystals were obtained as follows. We first calculated the plagioclase-melt partition coefficients using the measured An contents and the equations of ref. 8. Using the partition coefficients, and the measured trace element concentrations at the crystal rims, we then calculated a melt composition in equilibrium with the rim. Finally, the composition of the entire plagioclase crystal in equilibrium with the calculated melt (and crystal rim) was calculated using the partition coefficient for each portion of the crystal.

The *initial* Mg profile was estimated using the Sr-An correlation of Fig. 3c and the Mg-Sr liquid line of descent (Fig. 3b). The relationship between the initial Mg and An contents used in the modelling is: ppmMg = 48.2 exp[2.9 *XAn*]. This approach is justified because the times involved in the processes are short enough not to have affected Sr concentrations in any significant manner. The uncertainty in the initial Mg content shown in Fig. 2 was estimated by error propagation. For the *boundary conditions* we used measured concentrations at the rims of the crystals or at the appropriate boundary between two crystal zones in the multiple step models.

In the modelling we explored two end-member possibilities. (1) Model the entire crystal including the rim, core, and calcic inner core all at once (1-step model) at 900 °C. This is like assuming that diffusion started only after the crystal was fully grown, and is the approach of all previously published models using plagioclase.

This should not be a bad approximation if the diffusion time is relatively long and if growth rates are relatively high. (2) Model the crystal by pieces; for example, first model equilibration of the calcic inner core with either 900 °C dacitic melt or with the crystal core and the dacitic melt, then add the rim and 855 °C rhyodacitic melt and continue diffusing (2-step model). This is a first-order approximation for modelling simultaneous crystal growth and diffusion. We have tried both approaches, and in most cases there are no significant differences in total times, but the fits to the data are better if we use the 2-step approach. This also gives us additional information about the timescales of different processes recorded in different parts of the crystals. To our best knowledge this is the first time that plagioclase zoning has been used to provide chronologies of multiple events from single crystals. It is interesting to see that, in order to successfully model some crystals, we need to use a condition where Mg in the crystal was already equilibrating with the host melt before any subsequent overgrowth by a new composition.

We illustrate the two approaches using crystal S82-30A 12 (Fig. S5). We were not able to obtain a good fit to the measured Mg profiles using a 1-step model, which gave an approximate time of 47 years. We therefore modelled the diffusion using the 2-step approach. We first did an inner-core/core/melt equilibration at 900 °C, and obtained a time of 70 years (step 1 of Fig. S4b). We then added the rim over the core, continued to diffuse at 855 °C, and obtained a further time of 12 years (step 2 of Fig. S4b). The total time recorded by the crystal is therefore 82 years, with a fit that is clearly better than with a 1-step approach. We also tried more detailed models involving, for example, 3 steps (inner-core/melt, inner-core/core/melt, and inner-core/core/rim/melt, but the results were virtually identical to the 2-step model.

In the case of the rimless type-1 crystal (S82-11D A5), the composition of which is out of equilibrium with the host rhyodacitic melt, we modelled the time necessary for Mg and Sr in the outer 25 μm of the crystal to be significantly modified by diffusive re-equilibration. The times at 855 °C were 0.3 years for Mg (Table 1) and 12 years for Sr. The crystal therefore cannot have resided in the melt for longer than 0.3 years.

The times obtained from Mg diffusion calculations are subject to various types of uncertainties[7]. First, the temperatures obtained from geothermometers have errors of about $\pm$25 ^{o}C, which when propagated onto the time estimates lead to the relative uncertainties given in Table 1. Second, the diffusion calculations were carried out in 1D, which has been shown to overestimate actual (3D) diffusion time[7] when the extent of diffusion is as significant as that shown by some of the inner cores of our crystals. Third, uncertainty arises from experimentally determined diffusion coefficients. Mg diffusion in plagioclase[28] was measured on An_{95} and at 1200-1400 °C, and the measurements are precise to within a factor of two. Following ref 12, equation S1 assumes that the activation energy and pre-exponential factor determined for D_{Mg} at higher temperatures applies at 900 °C. Down-temperature extrapolation of diffusion data is common practice, and a necessity for almost all studies that use experimentally determined diffusion coefficients to model natural processes[35,36]. This is because the experimental times required to produce significant profiles to determine Ds are impossibly long (but see ref 37) . The extrapolation is not a significant problem if there is no change of the diffusion mechanism (which would imply a change in the activation energy) at lower temperatures. There have been many determinations of

other cation diffusivities (e.g., Sr, Li, Ca[38]) in plagioclase feldspars at a wide ranges of temperatures (including 900 °C), and these do not show kinks in activation energy.

There is also uncertainty on the An dependence in equation S1, which assumes that the An dependence of Mg diffusion is the same as that of Sr[12]. This assumption was used in ref 12 because only certain dependencies are possible to obtain good fits to the natural data. In addition to this observation, we have here estimated an uncertainty due to the An dependence term in equation S1 by combining natural data and the well calibrated Sr diffusivities. The data in Table 1 and Fig. 2, as well as that published elsewhere [7,39,40], show that the degree of equilibration of Mg is always higher than that of Sr, irrespective of An content. This means that $D_{Mg} > D_{Sr}$ not only for An_{95} (ref 28), but for all An contents. Thus, the dependence of D_{Mg} on An can not be too low because otherwise $D_{Sr} > D_{Mg}$ at low An. Using this constraint, and equation S2 for D_{Sr}, the minimum possible dependence of An has the form of $(-2.6X_{An} -4.53)$ in equation S1, which is a much lower slope (Fig. S6). The effect that this has on the times ranges from a factor of two longer for the 1-step fit for crystal R2C B3 (130 years), to a factor of three longer for crystal 34BA2 (2.3 years). We conclude that the uncertainty in this parameter does not increase the times in Table 1 by more than about a factor of three.

We also carried out diffusion modelling of Sr (for which the diffusion parameters are very well constrained[29]; Fig. 2), in order to gain first-order independent constrains on the timescales inferred from Mg. For this we assumed that the observed profiles were near-primary and carried out 1-step diffusion models at 900 °C to see what times were required for significant perturbation of those profiles. The results (Fig. 2) show that crystal residence times longer than a couple of hundred years would significantly blur the tight relationship between plagioclase Sr and An content (Fig. 3c), and are therefore excluded.

Finally, there is also an uncertainty on the determination of the best fits of the model and measured concentrations, which include the analytical errors. The fits were done visually because, given the complexity of the natural profiles, it doesn't make sense to implement least-squares routines. The uncertainty from this varies from crystal to crystal, and ranges from less than 10% for crystals that have been largely equilibrated (eg., step 1 of most crystals) to up to 40 % for step 2, where concentrations vary by a small amount and may be close to the initial values (e.g., crystal S82-34B A2).

References

31. Hinton, R.W. Ion microprobe trace-element analysis of silicates: Measurement of multi-element glasses, *Chemical Geology* **83**, 11-25 (1990).
32. Vaggelli, G., Pellegrini, M., Vougioukalakis, G., Innocenti, S. & Francalanci, L. Highly Sr radiogenic tholeiitic magmas in the latest inter-plinian activity of Santorini volcano, Greece. *J. Geophys. Res.* **114**, BO6201 (2009).
33. Conticelli, S., Francalanci, L., Santo, A.P. & Petrone C. Petrographic, chemical and isotopic variations in the intra-caldera post-Minoan rocks of the Santorini volcanic field. *Proceedings of the second workshop, Santorini, Greece, European Commission* pp157-174 (1998).
34. Gertisser, R., Preece, K. & Keller, J. The Plinian Lower Pumice 2 eruption, Santorini, Greece: Magma evolution and volatile behaviour. *J. Volcanol. Geotherm. Res.* **186**, 387-406 (2009).
35. Lasaga, A.C. Kinetic theory in the earth sciences. Princeton University Press. 817 pp (1998).

36. Zhang, Y. Diffusion in minerals and melts: Theoretical background. *Rev. Mineral. Geochem.* **72**, 5-59 (2010).
37. Chakraborty, S., Dohmen, R., Becker, H.W., Meissner, E. & Etzel, T. Production of silicate thin films using pulsed laser deposition (PLD) and applications to studies in mineral kinetics. *Eur J Mineral* **14**, 1155-1168 (2002).
38. Cherniak, D. Cation diffusion in feldspars. *Rev. Mineral. Geochem.* **72**, 691-733 (2010).
39. Costa, F., Coogan, L. & Chakraborty S. The time scales of magma mixing and mingling involving primitive melts and melt–mush interaction at mid-ocean ridges. *Contrib. Mineral. Petrol*. **159**, 371–387 (2010).
40. Costa, F. & Morgan D. Time constraints from chemical equilibration in magmatic crystals. In *Timescales of magmatic processes: from core to atmosphere* (eds Dosseto, A., Turner, S.P. & Van Orman, J.A), 125-159 (Wiley-Blackwell, 2010).

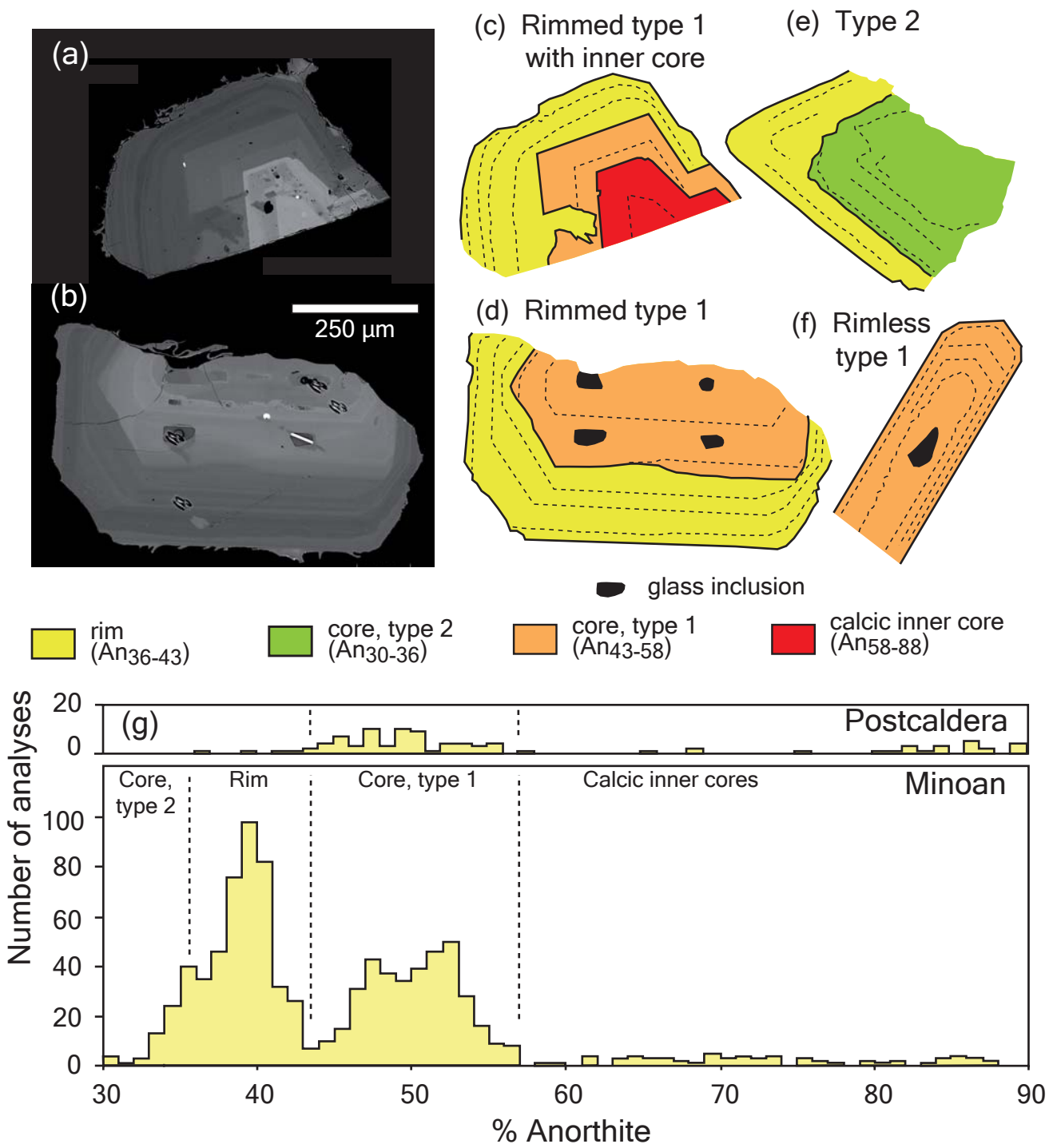
(a)
(b)
250 µm
(c) Rimmed type 1 with inner core
(e) Type 2
(d) Rimmed type 1
(f) Rimless type 1
glass inclusion
rim (An36-43)
core, type 2 (An30-36)
core, type 1 (An43-58)
calcic inner core (An58-88)
(g)
Postcaldera
Minoan
Core, type 2
Rim
Core, type 1
Calcic inner cores
Number of analyses
% Anorthite
0
20
40
60
80
100
30
40
50
60
70
80
90

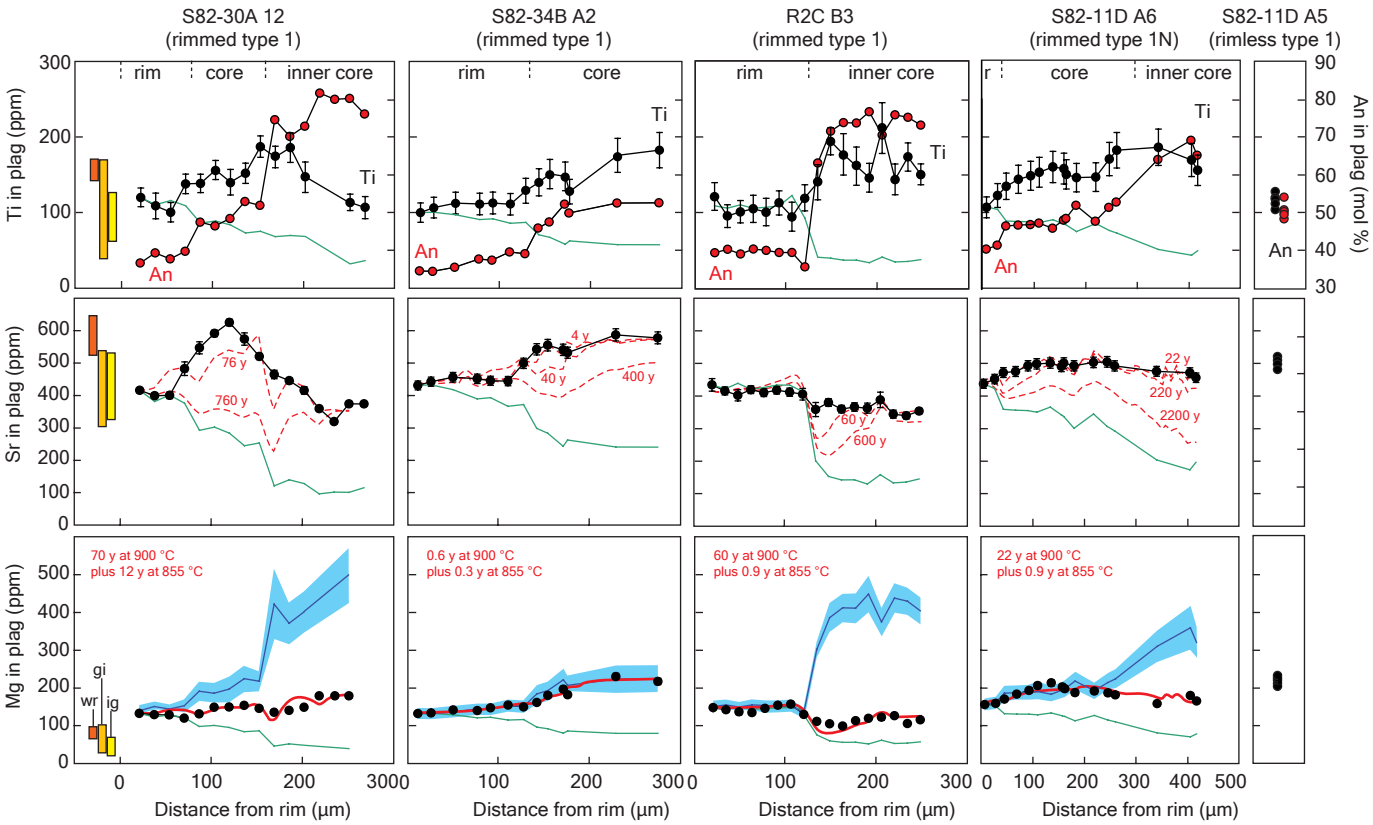
S82-30A 12
(rimmed type 1)
S82-34B A2
(rimmed type 1)
R2C B3
(rimmed type 1)
S82-11D A6
(rimmed type 1N)
S82-11D A5
(rimless type 1)
rim
core
inner core
Ti
An
Ti in plag (ppm)
An in plag (mol %)
Sr in plag (ppm)
76 y
760 y
4 y
40 y
400 y
60 y
600 y
22 y
220 y
2200 y
Mg in plag (ppm)
70 y at 900 °C
plus 12 y at 855 °C
0.6 y at 900 °C
plus 0.3 y at 855 °C
60 y at 900 °C
plus 0.9 y at 855 °C
22 y at 900 °C
plus 0.9 y at 855 °C
gi
wr
ig
Distance from rim (µm)

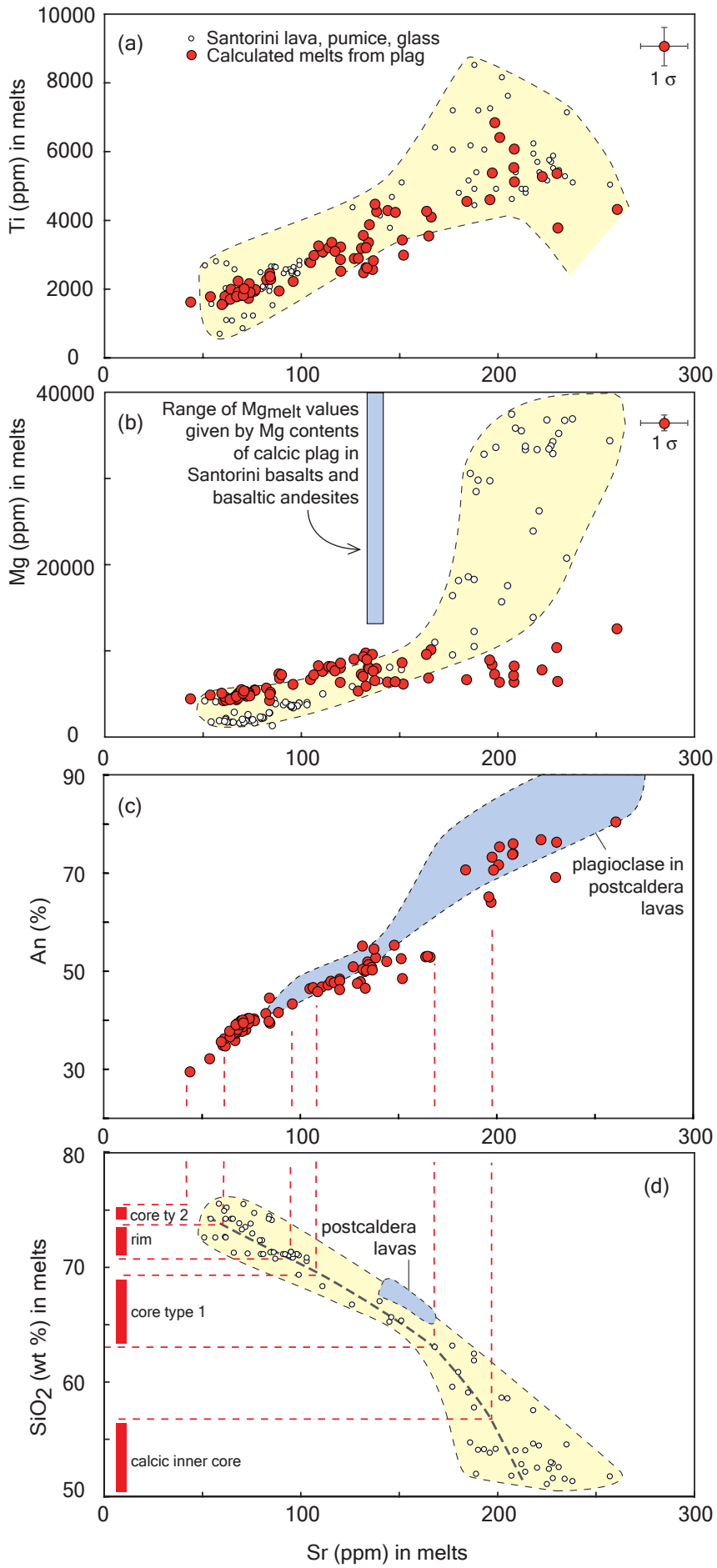
(a)
Santorini lava, pumice, glass
Calculated melts from plag
1 σ
Ti (ppm) in melts
10000
8000
6000
4000
2000
0
0
100
200
300
(b)
Range of Mgmelt values given by Mg contents of calcic plag in Santorini basalts and basaltic andesites
1 σ
Mg (ppm) in melts
40000
20000
0
0
100
200
300
(c)
plagioclase in postcaldera lavas
An (%)
90
70
50
30
0
100
200
300
(d)
core ty 2
rim
core type 1
calcic inner core
postcaldera lavas
SiO2 (wt %) in melts
80
70
60
50
0
100
200
300
Sr (ppm) in melts

SUPPLEMENTARY INFORMATION

1. Supplementary Figures

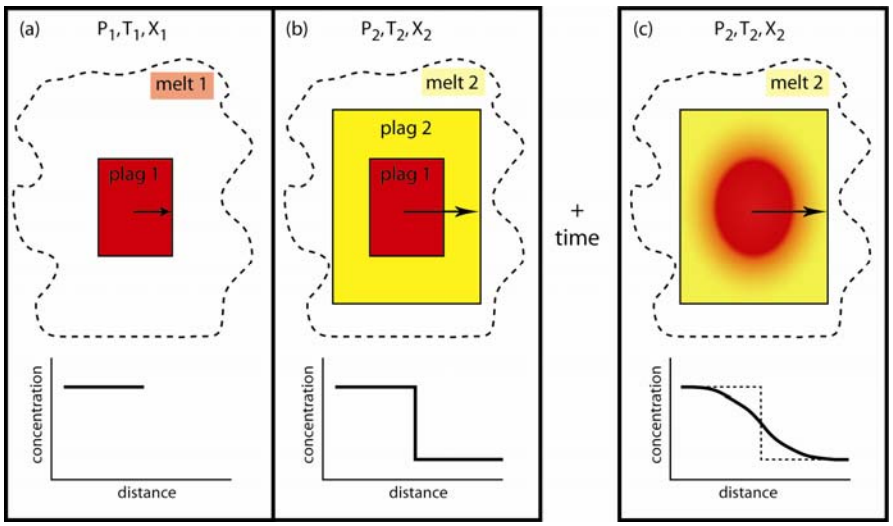

Figure S1 : Schematic figure showing a crystal growing from a melt with a given set of variables (P: pressure, T: temperature, X: composition). The arrows show traverses corresponding to the compositional profiles in each case. (a) A plagioclase crystal of composition plag 1 grows from melt 1 under one particular set of conditions. (b) The crystal is transferred by magma mixing to another melt, melt 2, and is overgrown by plagioclase of composition plag 2 in equilibrium with melt 2. (c) If the crystal then sits in melt 2 for long enough, diffusion will tend to smooth out the compositional step between the two crystal zones. Major element diffusion in plagioclase (the exchange CaAl – NaSi) occurs very slowly on geological timescales, so that primary zoning of An content is nearly always preserved[40]. However, some trace elements diffuse fast enough in plagioclase to generate measurable intracrystalline diffusion gradients[7]. Slow-moving trace elements preserve primary values, and can be used to calculate the compositions of melts 1 and 2. Diffusion gradients generated by relatively fast-diffusing elements can be used to estimate the time between stages b and c in the diagram. Both approaches are exploited in this study.

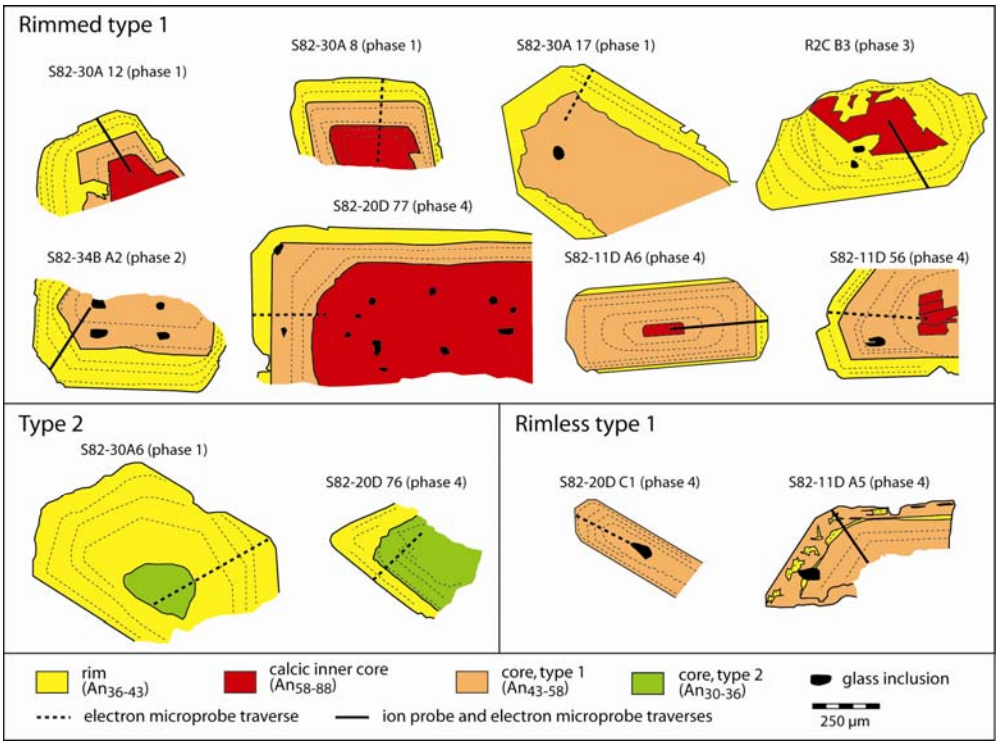

Figure S2 : Representative crystals of the different plagioclase types, with compositional traverses.

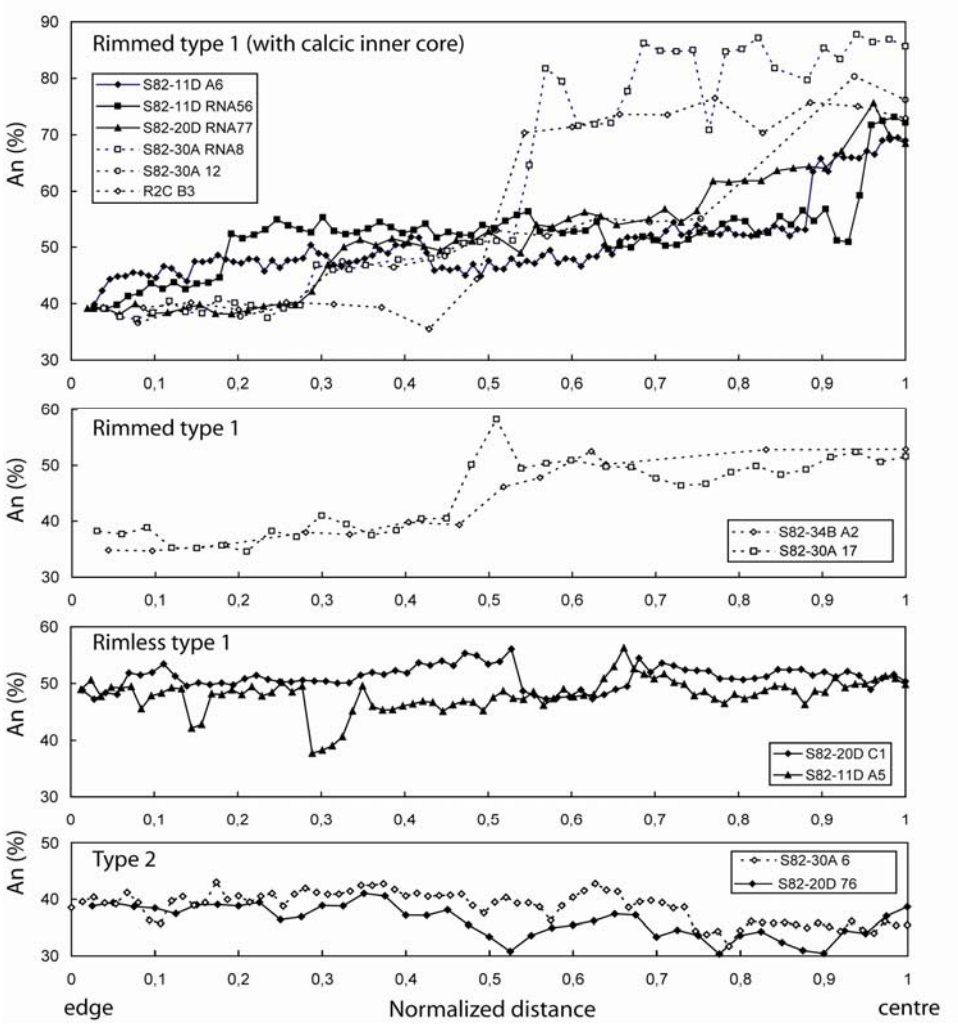

Figure S3 : Core-to-rim profiles of An content in the twelve representative plagioclase crystals shown in Fig. S2. The profiles were analysed by electron microprobe.

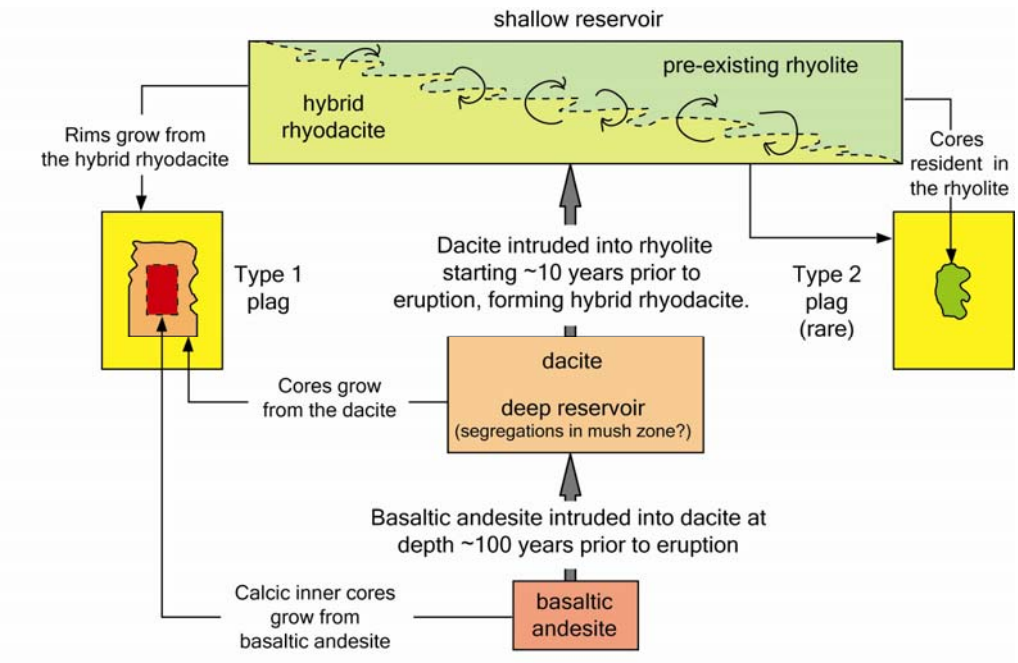

Figure S4 . Summary of magmatic processes and their time scales prior to the Minoan eruption, as determined from crystal zoning data, models, and other geological observations.

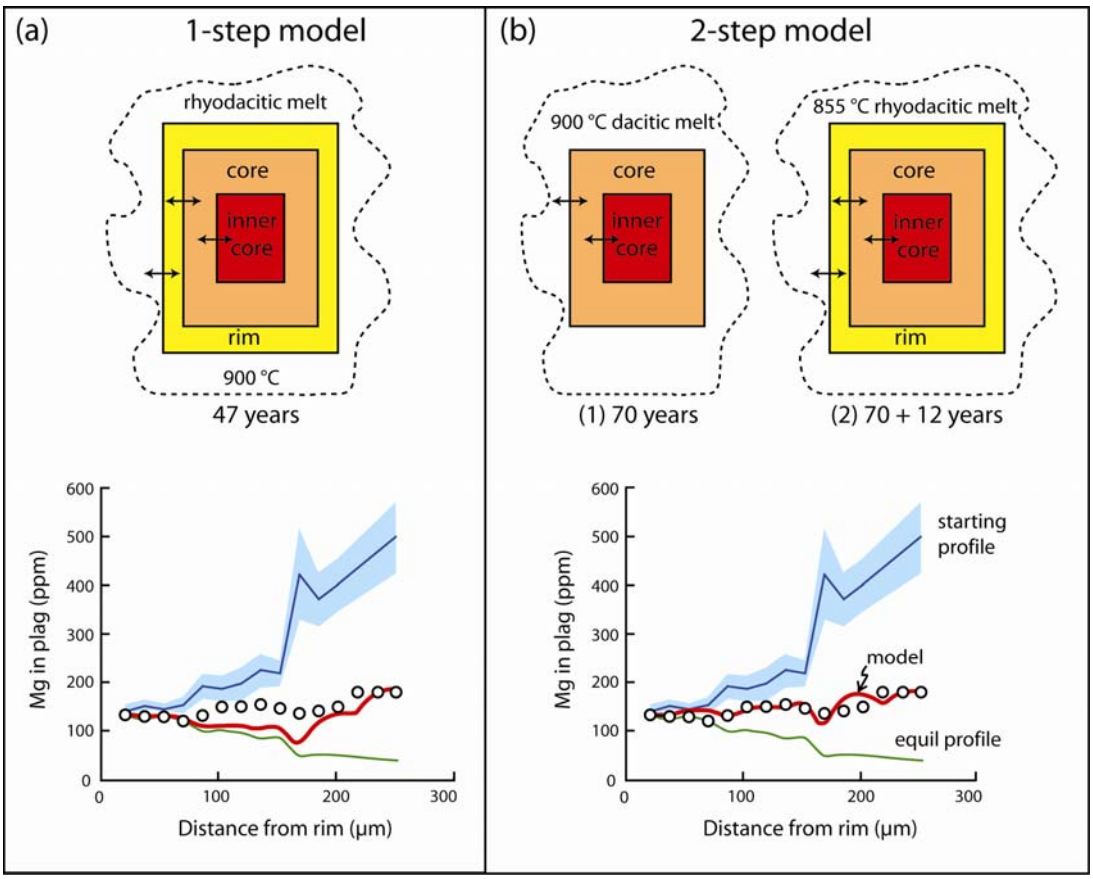

Figure S5: Explanation of the two modelling approaches taken in the study, using as example crystal S82-30A 12. (a) One-step diffusion model for Mg at 900 °C using a distance increment of 4.1 μm. The circles are the measured profile. The blue line is the estimated initial profile (with 1 σ error range), the green line is the equilibrium profile, and the red line is the model. A 1-step model at 900 °C gives a poor fit at about 47 years for the whole crystal. (b) The 2-step model, involving exchange between the calcic inner-core and the core at 900 °C (70 years) followed by exchange between the inner-core, core and rim at 855 °C (12 years), gives a much better fit. We also tried with three steps, but the fit did not improve and the time did not change.

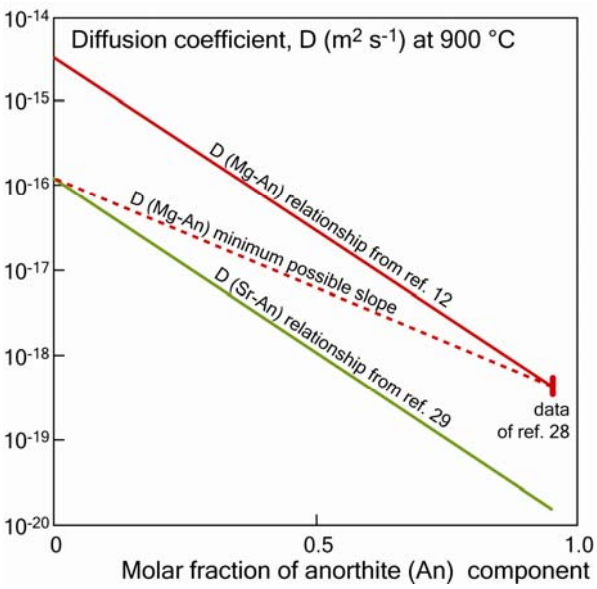

Figure S6. Plagioclase zoning patterns of natural crystals[7,39,40] show that Mg is more equilibrated than Sr at all anorthite contents. This requires that $D_{Mg}>D_{Sr}$ for all An. In the above plot we show that the minimum slope that characterises the dependence of the D_{Mg} with An is bounded by the experimental data for Mg of ref. 28 and that for Sr of ref. 29. Using this minimum slope we obtain times that are only about a factor of 2 to 3 longer than those we report in Table 1.

2. Supplementary Tables

Table S1. Trace element contents of Minoan plagioclase phenocrysts

Pumice	Crystal	Distance from rim (µm)	An (mol %)	Mg (ppm)	K (ppm)	Ti (ppm)	Sr (ppm)	Ba (ppm)	La (ppm)	Ce (ppm)
S82-11D	**A6**	9	40.2	155	2293	108	435	224	9.03	8.86
		31	41.3	158	2181	123	450	198	8.02	7.94
		47	46.3	170	1917	135	470	163	7.28	6.46
		71	46.6	183	1780	144	473	141	6.44	6.16
		94	46.7	193	1774	149	491	136	6.13	5.84
		111	47.1	206	1767	154	497	128	5.97	5.87
		137	45.8	213	1892	161	499	131	6.02	5.97
		158	47.9	202	1719	159	489	129	5.91	5.91
		163	48.3	197	1655	151	499	126	6.13	5.65
		182	51.8	187	1582	147	491	116	5.35	5.23
		220	47.6	191	1647	147	501	119	5.54	5.09
		246	51.2	186	1542	171	503	107	5.04	5.08
		260	52.7	181	1446	183	491	102	4.80	4.43
		340	63.9	158	1503	187	474	71	2.59	2.66
		404	69.0	179	1208	170	470	69	2.91	2.90
		416	65.0	165	1411	156	454	89	3.95	3.46
S82-11D	**A5**	5	49.9	233	1406	119	522	152	8.28	7.94
		48	50.7	226	1453	115	519	162	8.29	7.71
		117	47.9	212	1577	119	507	150	6.91	6.87
		194	50.8	212	1429	129	482	147	6.47	7.45
		231	41.5	204	2049	105	480	201	8.50	8.65
		291	50.3	221	1735	111	509	152	7.76	7.92
		377	50.1	214	1522	118	520	157	8.35	8.27
S82-34B	**A2**	12	34.8	133	2987	100	431	344	9.63	8.24
		27	34.7	134	3066	106	442	349	9.95	8.65
		51	35.8	142	2954	112	456	383	9.60	8.52
		77	38.0	141	2923	111	451	379	9.50	8.43
		92	37.7	148	2711	113	445	305	9.95	8.75
		111	39.8	155	2427	111	444	254	9.60	8.30
		128	39.4	150	2484	129	499	342	10.48	9.08
		142	46.1	162	1819	140	542	179	7.76	7.04
		154	47.8	181	1685	151	555	167	7.17	6.88
		171	52.5	197	1549	148	540	126	6.51	6.07
		176	50.1	182	1827	128	531	185	8.88	8.82
		229	52.8	230	1470	176	587	143	5.80	5.80
		275	52.8	217	1226	182	577	105	5.44	4.58
S82-30A	**B5**	5	37.3	130	2691	105	431	268	9.80	9.87
		16	37.3	137	2563	106	431	263	8.93	8.84
		24	37.5	142	2441	104	425	248	8.43	8.98
		41	38.9	146	2429	105	428	245	9.77	9.39
		59	39.3	149	2360	102	428	241	9.03	9.01
		78	38.6	145	2481	104	430	246	8.71	8.55
		97	38.9	149	2355	104	416	230	8.59	8.49
		122	39.6	149	2361	105	422	235	8.96	8.21
		157	36.2	144	2737	108	412	251	8.57	8.20
		211	38.1	149	2565	130	422	243	8.65	8.37
		230	39.0	153	2311	105	413	230	8.52	8.90
		246	39.8	158	2322	108	403	244	9.32	9.48
		273	29.4	155	3746	114	393	322	11.15	10.64
		302	32.1	161	2854	118	430	272	10.05	9.77
		359	43.2	165	2063	116	485	198	8.10	7.33
S82-30A	**12**	21	36,6	133	2741	117	416	285	8,33	12,02
		38	39,3	130	2418	107	400	257	7,70	7,55
		54	37,7	129	2420	99	401	249	6,12	9,69
		71	39,7	120	2362	136	483	256	8,51	6,58
		87	47,4	131	1997	136	548	255	5,69	8,16
		103	46,4	149	1737	155	592	194	5,99	7,25
		120	48,4	150	1860	139	626	194	4,35	7,09
		136	52,9	154	1567	150	575	167	3,77	6,06
		153	51,9	146	1340	185	521	117	2,22	4,85
		169	74,6	136	718	168	465	48	2,11	3,07
		185	70,2	141	804	181	446	72	2,18	3,45
		202	72,9	149	816	142	416	59	4,12	5,84
		218	81,7			118	360	74	1,83	3,33
		235	80,1				320	49	3,44	5,22
		251	80,3	179	655	112	375	42	1,19	2,85
		267	76,2	98	560	105	374	28	1,40	1,50
R2C	**B3**	21	39,4	148	2380	122	434	242	7,23	10,53
		35	40,3	143	2583	96	415	225	6,71	10,52
		49	39,0	137	2489	102	402	232		7,11
		64	40,3	135	2654	105	419	246	8,36	8,73
		78	39,9	147	2442	102	410	261	5,85	9,78
		92	39,4	155	2554	113	418	233	5,48	9,00
		106	39,4	158	2599	95	412	248	7,52	8,88
		120	35,6	130	2865	120	406	245	5,53	7,80
		134	63,1	112	1351	140	358	121	3,68	4,24
		148	71,5	106	872	195	380	76	2,02	1,83
		163	73,8	100	649	174	360	35	0,00	0,53
		177	73,7	114	793	161	366	36	0,55	0,60
		191	76,7	120	757	148	363	26	0,52	1,13
		205	70,5	123	827	212	388	21	0,57	1,24
		219	75,9	127	780	144	344	23	0,58	1,27
		233	75,2	106	762	174	340	39	0,40	0,44
		247	73,1	116	841	150	354	39	0,77	0,28

Table S2. Trace element contents of Minoan glasses

Pumice	Crystal	SiO2 (wt %)*	Mg (ppm)	K (ppm)	Ti (ppm)	Sr (ppm)	Ba (ppm)	La (ppm)	Ce (ppm)
Interstitial glasses									
S82-30A	A4	73.9	1876	28153	1802	74	679	28.5	48.3
S82-30A	A4	73.6	1858	28317	1807	72	616	27.0	44.4
S82-30A	12	74.5	2786	22627	2070	84	566	38.4	57.2
S82-34B	A8	74.2	1308	26992	1528	85	606	30.8	53.3
S82-34B	A9	73.9	1624	29522	1737	69	678	32.4	59.0
R1C	4	74.8	1633	32002	1879	76	656	30.5	55.7
R1C	4	74.3	1713	27953	1086	65	596	29.6	48.6
R1C	27	74.3	1747	26205	1567	54	524	28.8	53.0
R1C	27	74.3	2169	26100	1100	62	521	27.7	54.4
R2C	B3	74.3	1712	30888	1906	65	654	25.1	47.6
S82-11D	D1	74.3	2809	32132	1944	84	657	31.0	60.1
Glass inclusions									
S82-30A	3	72.7	2029	29510	2024	61	594	29.2	53.3
R1C	3	73.0	2003	34822	1228	75	712	33.1	67.3
R1C	3	75.6	1688	32135	1226	71	640	29.6	56.0
R1C	17	73.4	2050	29243	859	70	642	32.8	64.0
R1C	17	75.3	1736	27865	1871	62	642	25.5	74.5
R1C	27	75.6	1892	26597	702	58	521	32.2	50.2
R1C	27	75.0	1826	27950	1640	61	533	33.3	43.4
S82-34B	11	71.2	2141	30500	1998	80	615	40.3	55.8
S82-34B	11	71.2	2220	30500	2042	81	620	40.9	57.9
S82-34B	11	72.4	2263	32183	2073	80	626	41.5	57.0
S82-34B	11	72.4	2320	31098	2487	79	635	40.1	55.8
S82-11D	A5	72.7	4202	26205	2686	51	596	37.0	55.8
S82-11D	A5	72.7	4091	30050	2808	57	816	52.6	68.7
S82-11D	A5	72.7	4246	30643	2745	62	847	52.8	70.9
S82-11D	A5	71.4	4250	31320	2656	85	840	52.8	68.5
S82-11D	A5	71.4	4341	31320	2656	86	864	55.2	68.9

* from electron microprobe analysis

Table S3. Parameters used in the calculations of mixing time and efficiency

Symbol	parameter	value
Gravitational acceleration	g	$9.8\ m\ s^{-2}$
Chemical diffusivity	D	$10^{-13}\ m^2\ s^{-1}$
Density of ambient fluid (rhyolite)	ρ_a	$2300\ kg\ cm^{-3}$
Density of input fluid (dacite)	ρ_i	$2350\ kg\ cm^{-3}$
Coefficient of thermal expansion	α	$3 \times 10^{-5}\ K^{-1}$
Thermal diffusivity	κ	$8 \times 10^{-7}\ m^2\ s^{-1}$
Viscosity of rhyolite	η_a	10^4 Pa s
Viscosity of dacite	η_i	10^3 Pa s
Kinematic viscosity of rhyolite	ν_a	$4.25\ m^2\ s^{-1}$
Kinematic viscosity of dacite	ν_i	$0.44\ m^2\ s^{-1}$
Thickness of the rhyolite layer	H	0.7-1 km
Flux per unit area of input fluid (dacite)	V_i	$0.05\ km^3\ y^{-1}$

3. Supplementary Discussion

Evidence for the dacitic magma component

A key feature of our interpretation is that the cores of the type-1 plagioclase crystals crystallized from dacitic magma on the timescales given by our diffusion modelling. An alternative possibility is that they (and the included calcic inner cores) were recycled from old plutonic mush in which they had been stored for long times at temperatures sufficiently low to prevent re-equilibration of trace elements. Defrosting of pre-existing bodies of plutonic mush by intrusion of hotter magma has been postulated as an important process for generating eruptions of crystal-rich intermediate to silicic magmas[41-43]. In this hypothesis our decadal timescales would record the duration of defrosting of the mush[6,44,45] prior to eruption. However, we do not favour this hypothesis, for the following reasons. First, crystals in the Minoan magma occur individually, and crystal clusters expected to form by disaggregation of low-temperature mush are rare. Second, the presence of euhedral, rimless type 1 crystals (with the same An contents as the cores of the rimmed type-1 crystals) strongly suggests that dacitic magma was present in the Minoan plumbing system at a late stage prior to eruption. Third, the Minoan magma contains only ~10 vol% crystals, so a very large degree of remelting would be required to generate it by reactivation of a low-temperature mush. Fourth, discharge of dacitic immediately followed the Minoan eruption in the form of the postcaldera lavas[13,16,46].

Identities of the dacitic and rhyolitic magmatic components

The dacite is inferred to have been a vanguard batch of the magma discharged during the postcaldera eruptions[16,46], for the following reasons. First, plagioclase phenocrysts in the postcaldera lavas have the same ranges of An and Sr contents as the cores of the Minoan type-1 crystals (Fig. 1g). Second, the $^{87}Sr/^{86}Sr$ ratios of the interiors of the Minoan plagioclases are lower than those of Minoan glass[15], but are overlap with those of the postcaldera lavas[16]. Third, the postcaldera magma was erupted immediately following the Minoan eruption, showing that it was available at depth in the plumbing system. We interpret the postcaldera activity as the continuation of an event of magma transfer from depth that preceded, and perhaps initiated, the Minoan eruption.

The identity of the rhyolitic component is less tangible. No lavas, and no layers of silicic pumice, are preserved between the Minoan products and those of the preceding large explosive eruption of Santorini (22 ka)[13]. The only pyroclastic unit is a small scoria fall deposit[32]. Despite detailed sampling, we have not found any blocks of lava in the Minoan deposits that could be samples of extruded pre-Minoan rhyolite. We believe the rhyolite to be possibly related to a suite of crystal-rich pumices and plutonic nodules that are a volumetrically minor (typically a few %) component of the Minoan deposits[13]. They are concentrated in the Plinian fall deposit of the first eruptive phase, but were also discharged in trace quantities in the other three phases. They have whole-rock silica contents ranging from 53 to 63 wt %, crystal contents from 55 to >95 vol%, and rhyolitic (72-77 % SiO_2) interstitial glass. The mineral assemblage is plagioclase, orthopyroxene, clinopyroxene, magnetite, and some samples also contain ilmenite and hornblende. Touching pairs of Fe-Ti oxides yield[26,27] temperatures of 770-830 °C and fO_2 ~NNO. The high Ba contents and $^{87}Sr/^{86}Sr$ ratios of the

crystal-rich pumices and plutonic nodules rule out that they formed by crystal accumulation from Minoan rhyodacite[13,15]. They are interpreted as samples of the crystalline carapaces of one or more bodies of cool, oxidized, and crustally contaminated rhyolite that were present in the upper crust beneath Santorini prior to the Minoan eruption. We speculate that intrusion and mixing of dacite into these rhyolitic bodies on the timescales described in this paper led to the formation of the large, shallow[14] reservoir of hybrid rhyodacite that was then discharged during the Minoan eruption. The dacitic magma could have been derived by rapid draining from a plexus of long-lived storage zones in a mushy pluton deeper in the crust.

Mixing proportions of the silicic magmas

The mixing proportions of dacite and rhyolite in the Minoan magma can be estimated approximately using the Sr_{melt} values of Fig. 3d for the three different components (dacite 110-170 ppm, rhyolite 40-60 ppm, hybrid rhyodacite 60-90 ppm). Taking extreme values, simple mass balance yields a proportion of dacite ranging from 15 to 40 %, which, for a total rhyodacite volume of 40-60 km^3 (ref 4), corresponds to a volume of the dacitic mixing component of 5-25 km^3.

This estimate is broadly consistent with the abundance of dacite-derived plagioclase (cores of the type-1 crystals) observed in the hybrid rhyodacite. The rhyodacite contains ~10 % crystals, of which ~7 % are plagioclase. Of this plagioclase, the dacite-derived cores account for very roughly half (Fig. 1g). Assuming that the intruding dacite contained between 10 % (plagioclase content of the postcaldera lavas[16,17]) and 50 % (roughly the maximum crystal content permitting flow), then simple crystal conservation places the percentage of the dacitic mixing endmember as 7-35 %, which is similar to range estimated above.

We conclude conservatively that perhaps a few km^3 of dacite was injected into the Minoan reservoir during the ~100 years prior to eruption.

Fluid dynamic constraints on mixing timescales

The 40-60 km^3 of Minoan magma is homogeneous in whole-rock composition (71-72 % SiO_2), glass composition (73-74 % SiO_2), and Fe-Ti oxide temperature (853$\pm$12 °C), irrespective of eruptive phase. The only heterogeneity we have found is a concentration of rimless type-1 crystals in pumices of eruptive phase 4. Clearly the mixing of dacitic and rhyolitic magmas inferred to have taken place on timescales ranging from ~10 years to a few months must have been very efficient to result in such homogeneity. We have therefore tested whether efficient mixing on these timescales is compatible with the physics of magma mixing, using the results of ref 47 to evaluate under what fluid dynamical conditions mixing is efficient between two fluids of different viscosities and densities. The two relevant non-dimensional variables in such a context are the Reynolds number (Re) and the ratio of the kinematic viscosities of input (ν_i) and ambient (ν_a) magmas, U :

$$U = \nu_a / \nu_I \qquad [S1]$$

The relevant Reynolds number[47] is:

$$Re = B^{1/3} H^{4/3}/\nu_a$$

where B is the buoyancy flux, H the thickness of the layer of ambient fluid (rhyolite) and ν_a its kinematic

viscosity. The buoyancy flux is calculated as:

$$B = gV_i (\rho_a-\rho_i) / \rho_a \qquad [S2]$$

where g is the gravitational acceleration, V_i is the flux per unit area of input fluid (dacite), ρ_a is the density of the ambient fluid, and ρ_i the density of the input fluid. Values used for the calculations are listed in Table S3.

As with any mixing phenomenon, the viscosity contrast between the two fluids plays a key role. In our case, the viscosity of both fluids can be evaluated using petrological constraints on T-H_2O_{melt} coupled to viscosity models[48]. Mineral thermobarometry[46] and phase equilibrium constraints available for similar compositions[49,50] show that the intruding dacite was at 900-950°C and contained ~4 wt% dissolved H_2O. Application of viscosity models yields a dacite melt viscosity (η_i) around 10^3 Pa s. For the rhyolite end-member we lack precise melt compositions, but we assume a melt with 71-72 wt% SiO_2 and 5-6 wt% water. The crystal-poor character of the resulting hybrid rhyodacite dictates that both mixing components were also crystal-poor, which implies a temperature of ~830°C for the rhyolite. This in turn yields a viscosity of about 10^4 Pa s for the rhyolite (η_a), in agreement with previous work for other silicic arc magmas[51]. Thus, the ratio of kinematic viscosities U was less than 10. Calculation of the convective Reynolds number gives a value of 750. Note that we use a magma flux of 0.05 km^3/year, which is a conservative estimate; increasing the flux by 1-2 order of magnitude will increase the Re well beyond 1600. These two parameters indicate a mixing efficiency higher than 0.95, following the results of ref 52 (perfectly mixed systems having a value of unity), which shows that the system was thoroughly stirred, in agreement with the homogeneous character of the rhyodacitic magma ultimately erupted.

The mixing timescale can be inferred from published numerical simulations[53,54]. The relationships between strain rate ε, the layer thickness H across which convective motions occur, and the mixing timescale, T_m, are:

$$T_m = (1/2\varepsilon) \log (\varepsilon H^2/D) \qquad [S3]$$

where D is the chemical diffusivity of interest (taken here to be that of Si, one of the slowest diffusing species in silicate melts). The strain rate is given by:

$$\varepsilon = (0.023\ \kappa/H^2)\ Ra^{\ 0.685} \qquad [S4]$$

where κ is the thermal diffusivity, and Ra the thermal Rayleigh number defined as :

$$Ra = (\rho_a\ \alpha\ \Delta T\ g\ H^3)/ (\kappa\ \eta_a) \qquad [S5]$$

where α is the coefficient of thermal expansion of the fluid, ΔT the temperature gradient across the fluid layer of thickness H, and η_a the viscosity of the ambient fluid.

The effective thickness of the rhyolite can be estimated from the caldera area (~60 km^2) and magma volume (40-60 km^3)[4], which imply a thickness in the range 0.7-1 km. Using standard values for the input parameters (Table S3), such a range in thickness yields Rayleigh numbers in the range 10^{11}–10^{12} for a temperature drop ΔT of 10°C across the layer. This implies stirring times of less than 1 year, and possibly as short as 1 month (see also ref 54). Hence it appears that the physical estimate of the timescale of mixing is compatible with those inferred on petrological grounds. The efficiency of mixing at Santorini was greatly

facilitated by the near-liquidus nature of both magmas, as well as by the small difference in their respective viscosities.

Accommodation of the recharge volume

The intrusion of a few km^3 of magma into a shallow subvolcanic reservoir over about 100 years raises the question of how the volume was accommodated and what the surface manifestations and geophysical signals would have been. If accommodation took place purely through uplift, then huge surface deformations would be predicted. Assuming that the reservoir underlay the entire ~60 km^2 caldera, injection of a few km^3 of magma in a century would require surface uplift of several tens of metres, at rates approaching 1 m per year sustained for several decades, which is very large compared to historical rates of uplift at restless calderas[2,3]. For example, the uplift rate at Campi Flegrei between July 1982 and January 1985 reached 0.5 m/y, but was sustained for only two and a half years. Vertical uplift has been sustained for 700 years at Iwa Jima caldera, but at a mean rate of only 0.15-0.2 m/y^2. Another possibility is that some, or most, of the volume increase was accommodated by subsidence of the magma reservoir floor. Many granite plutons exhibit evidence for vertical growth by floor subsidence, either on faults or by downsagging[18,19,55]. Floor subsidence would compensate for rapid transfer of large volumes of magma from deeper in the crust, and could be essentially aseismic if faulting occurs beneath the brittle-ductile crustal transition or in plutonic mush[19]. Whether large surface uplifts and strong seismicity would necessarily have accompanied the pre-Minoan recharge events postulated at Santorini is in our opinion an open question. Archaeological evidence on Santorini has shown that seismic activity preceded the Minoan eruption by a few years to a few months[56,57], but it is not possible to say whether this had any causal relationship to the recharge events documented in this paper.

References

40. Grove T.L., Baker, M.B. & Kinzler R.J. (1984) Coupled CaAl-NaSi diffusion in plagioclase feldspar: experiments and applications to cooling rate speedometry. *Geochim. Cosmochim. Acta*. **48**, 2113-2121 (1984).
41. Nakamura, M. Continuous mixing of crystal mush and replenished magma in the ongoing Unzen eruption. *Geology* **23**, 807-810 (1995).
42. Murphy, M.D., Sparks, R.S.J., Barclay, J., Carroll, M.R. & Brewer, T.S. Remobilization of andesite magma by intrusion of mafic magma at the Soufriere Hills Volcano, Montserrat, West Indies. *J. Petrol.* **41**, 21-42 (2000).
43. Bachmann, O, Dungan, M.A. & Lipman, P.W. The Fish Canyon magma body, San Juan volcanic field, Colorado: Rejuvenation and eruption of an upper crustal batholith. *J. Petrol.* **43**, 1469-1503 (2002).
44. Bachmann, O. & Bergantz, G.W. Gas percolation in upper-crustal silicic crystal mushes as a mechanism for upward heat advection and rejuvenation of near-solidus magma bodies. *J. Volcanol. Geotherm. Res.* **149**, 85-102 (2006).
45. Huber, C., Bachmann, O. & Dufek, J. The limitations of melting on the reactivation of silicic mushes. *J. Volcanol. Geotherm. Res.* **195**, 97-105 (2010).
46. Barton, M. & Huijsmans, J. Post-caldera dacites from the Santorini volcanic complex, Aegean Sea, Greece: an example of the eruption of lavas of near-constant composition over a 2,200 year period. *Contrib. Mineral. Petrol.* **94**, 472-495 (1986).
47. Jellinek, A.M., Kerr, R.C. & Griffiths, R.W. Mixing and compositional stratification produced by natural convection. 1. Experiments and their applications to Earth's core and mantle. *J. Geophys. Res.* **104**, 7183-7201 (1999).

48. Giordano D., Russell J.K. & Dingwell D.B. Viscosity of magmatic liquids: a model. *Earth Planet. Sci. Lett.* **271**, 123–134 (2008).
49. Scaillet, B. & Evans, B.W. The 15 June 1991 eruption of Mount Pinatubo. I. Phase equilibria and pre-eruption P-T-fO_2-aH_2O. *J. Petrol.* **40**, 381-411 (1999).
50. Costa, F., Scaillet, B. & Pichavant, M. Petrological and experimental constraints on the pre-eruption conditions of Holocene dacite from Volcán San Pedro (36ºS, Chilean Andes) and the importance of sulphur in silicic subduction-related magmas. *J. Petrol*. **45,** 855-881 (2004).
51. Scaillet, B., Holtz, F. & Pichavant, M. Phase equilibrium constraints on the viscosity of silicic magmas 1. Volcanic-plutonic comparison. *J. Geophys. Res.* **103**, 27,257-27,266 (1998).
52. Jellinek, A.M. & Kerr, R.C. Mixing and compositional stratification produced by natural convection. 2. Applications to the differentiation of basaltic and silicic magma chambers and komatiite lava flows, *J. Geophys. Res.* **104**, 7203-7218 (1999).
53. Coltice, N. & Schmalzl, J. Mixing times in the mantle of the Earth derived from 2-D and 3-D numerical simulations of convection. *Geophys. Res. Lett.* **33**, doi : 10.1029/2006GL027707 (2006).
54. Huber, C., Bachmann, O. & Manga, M. Homogenization processes in silicic magma chambres by stirring and mushification (latent heat buffering). *Earth Planet. Sci. Lett.* **283**, 38-47 (2009).
55. Cruden, A.R. On the emplacement of tabular granites. *J. Geol. Soc Lond.* **155**, 853-862 (1998).
56. Doumas, C. Thera. Pompeii of the ancient Aegean. Thames and Hudson, 168pp (1983).
57. Marthari, M. The Destruction of the Town at Akrotiri, Thera, at the Beginning of LC I: Definition and Chronology. In *The Prehistoric Cyclades* (eds McGillivray, J.A & Barber, R.L.N), 119-133 (Dept. Classical Archaeology, Edinburgh, 1984).